Extrapolating fiber crossings from DTI data. Can we gain similar information as HARDI?

Conference Paper · January 2010

CITATIONS
6

READS
112

5 authors, including:

Vesna Prčkovska
Mint Labs
33 PUBLICATIONS **125** CITATIONS
SEE PROFILE

Bart ter Haar Romeny
Technische Universiteit Eindhoven
267 PUBLICATIONS **6,002** CITATIONS
SEE PROFILE

Anna Vilanova
Delft University of Technology
141 PUBLICATIONS **1,342** CITATIONS
SEE PROFILE

Extrapolating fiber crossings from DTI data.
Can we infer similar fiber crossings as in HARDI?

V. Prčkovska, P.R. Rodrigues, R. Duits,
B.M. ter Haar Romeny, and A. Vilanova

Department of Biomedical Engineering, Eindhoven University of Technology

Abstract. High angular resolution diffusion imaging (HARDI) has proven to better characterize complex intra-voxel structures compared to its predecessor diffusion tensor imaging (DTI). However, the benefits from the modest acquisition costs and significantly higher signal-to-noise ratios (SNRs) of DTI make it more attractive for use in clinical research. In this work we use contextual information derived from DTI data, to obtain similar fiber crossings as the ones recovered with the HARDI reconstruction techniques. We conduct a synthetic phantom study under different angles of crossing and different SNRs. We compare the extrapolated crossings from contextual information with HARDI data. We qualitatively corroborate our findings from the phantom study to real human data. We show that with extrapolation of the contextual information, the obtained crossings are similar to the ones from the HARDI data, and the robustness to noise is significantly better.

1 Introduction

The recent diffusion weighted magnetic resonance imaging (DW-MRI) technique, diffusion tensor imaging (DTI) [1], is subject of intense research mainly due to its feasibility in clinical practice (number of gradients (NG) around 20, b-value of 1000 s/mm^2 and total acquisition time of 3-5 minutes [2]). DTI constitutes a valuable tool to inspect fibrous structures in a non-invasive way. Despite the great potential for clinical applications, DTI has one obvious disadvantage due to the crude assumption for modeling the underlying diffusion process as Gaussian. In other words, in the areas of complex intra-voxel heterogeneity the DTI model fails to distinguish multiple fiber populations. This limits the accurate description of the diffusion process locally, and influences the accuracy of the fiber tracking algorithms, an important application of this model. To overcome the limitations of DTI, more complex acquisition schemes known as high angular resolution diffusion imaging (HARDI) were introduced [3]. These acquisitions come coupled with more sophisticated reconstruction techniques that tend to avoid any assumptions for the probability density function (PDF) that describes the underlying diffusion process. Thus, locally more accurate models for the diffusion process, that allow the detection of multiple fibrous structures, were introduced [4–9]. However, the increased accuracy in HARDI comes along with a few drawbacks, mainly in more time consuming acquisitions (60 to few hundreds NG, higher b-values ($> 2000\ s/mm^2$) and total acquisition times from 20 minutes to a few hours) [3,10]. This is one of the biggest impediments in applying

HARDI in a clinical setting. Another major issue is the SNR in the images acquired by the typical DTI or HARDI acquisition protocols for clinical scanners. Despite the more accurate local modeling of the underlying diffusion process by the HARDI techniques, they require acquisitions at higher b-values and denser gradient sampling compared to DTI. Therefore, the acquired datasets have significantly lower SNRs than in DTI (especially in the diffusion weighted images which is sometimes a factor of 4 lower). The reconstructed diffusion profiles suffer from major noise pollution that often produces false or displaced maxima of the reconstructed diffusion functions and might notably disturb the fiber tracking algorithms. Proper regularization techniques on the domain of these datasets are thus important. Moreover, there is an additional issue with the accuracy of the DW-MRI data. Since the noise is very prominent in the phase of an MRI signal, it is common to discard this information, thus considering only the amplitude. This results in anti-podally symmetric profiles as pointed out by Liu et al. [11], that can only model single fiber or symmetric crossings of multiple fibers. However, this can not always be assumed to be the case in the white matter of the brain, especially in structures such as *optic chiasm*, *the hippocampus*, *the brain stem* and others. Since the data is ill defined, considering the contextual information (i.e., neighborhood) can be of utmost importance. There has been previous work on inter-voxel, contextual based filtering for estimating asymmetric diffusion functions [12], and cross-preserving smoothing of HARDI images [13] by modeling the stochastic processes of water molecules (i.e., diffusion) in oriented fibrous structures. However, these approaches increase the complexity of already complex and computationally heavy HARDI data. Rodrigues et al. [14], accelerated these complex convolutions enabling a fast framework for the noise removal, regularization and enhancement of HARDI datasets. Notwithstanding, contextual processing as described above has been applied only on HARDI models, due to the natural coupling of the space of positions and orientations that describe the diffusion process.

In this paper, we address some of the above mentioned issues. We use data from typical clinically obtained DTI acquisitions to build orientation distribution functions (ODF) that can be used for contextual processing of the data. The data initially comes with high SNR values making the local reconstruction of the ODFs reliable. The context information of well defined single direction fibers is extrapolated to areas where the fiber structure is considerably complex and therefore not defined in DTI. We analyze the difference of the contextually modified ODFs compared with the Qball reconstructions [15] without any regularization from the same data as the estimated extrapolated ODFs (E-ODFs). To be fair, we extend this comparison to Qball's "best scenario" at high b-value ($3000 s/mm^2$) and dense gradient sampling (121 number of gradients) and with Laplace-Beltrami smoothing as reported in Descoteaux et al. [15]. We do quantitative analysis on synthetic crossings of two fibers at different angles and qualitative analysis on *in-vivo* data with the same acquisition as in the synthetic data. We come to a few interesting conclusions, suggesting that E-ODFs contain similar information as Qball's best scenario case. The E-ODFs could bring great

improvement to the DTI data, helping to overcome the limitations in crossing regions and enabling possibilities for streamline-based tractography.

2 Methods

In this section we present our method for creating extrapolated ODFs (E-ODFs) from diffusion tensors (DT) estimated from our DW-MRI data. We additionally give details on the contextual image processing and perform an evaluation.

2.1 Creating spherical diffusion functions from diffusion tensors

In DTI, the signal decay is assumed to be mono-exponential [16], and yields the equation:

$$S_g = S_0 \exp(-b\mathbf{g}^T\mathbf{D}\mathbf{g}) \tag{1}$$

where S_g is the signal in the presence of diffusion sensitizing gradient, and S_0 is the zero-weighted baseline signal, b is the b-value parameter of the scanner closely related to the effective diffusion time, and the strength of the gradient field, $\mathbf{g}$ are the diffusion gradient unit vectors, and $\mathbf{D}$ is the 2^{nd} order symmetric, positive definite diffusion tensor (DT). Once the DT is calculated per voxel, the orientation distribution function (ODF) can be reconstructed, and sampled on the sphere

$$ODF(\mathbf{n}) = \mathbf{n}^T\mathbf{D}\mathbf{n} \tag{2}$$

where $\mathbf{n}$ is the direction vector defined by the tessellation. Figure 1 shows a typical linear DT and the corresponding diffusivity profile sampled on a sphere (in our case icosahedron of order 4, 642 points on a sphere). Note that this ODF, since it is derived from the DT, does not hold any crossing information and should not be confused with the apparent diffusion coefficient (ADC) whose crossing information does not necessarily coincide with the underlying fiber population as pointed out by Özarslan et al. [7].

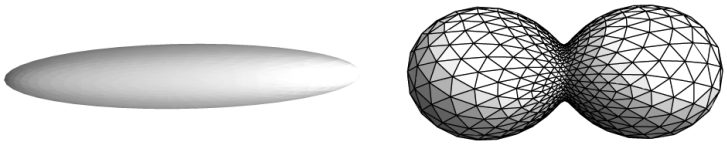

Fig. 1. A linear diffusion tensor (left) and the corresponding tessellated ODF (right).

From a tensor field we create an ODF field, i.e., a HARDI-like dataset $\mathcal{U}$ defined on the coupled space of positions and orientations [13], meaning the local diffusion profiles are defined not only spatially, but also as a function of orientation:

$$\mathcal{U} : \mathbb{R}^3 \rtimes S^2 \rightarrow \mathbb{R}^+ : \mathcal{U}(\mathbf{y}, \mathbf{n}(\beta, \gamma)) \tag{3}$$

This means that the probability density of a given water particle, starting at position $\mathbf{y}$, to have moved to a location with a certain direction $\mathbf{n}(\beta,\gamma)$ by the end of the diffusion time is given by by the scalar by the scalar $\mathcal{U}(\mathbf{y},\mathbf{n}(\beta,\gamma))$. Here, β and γ are not the standard spherical coordinates. They are parametrized via a different chart, as described in Duits et al. [13]. To stress the coupling between orientations and positions, that comes along with the alignment of fiber fragments, we write $\mathbb{R}^3 \rtimes S^2$ rather than $\mathbb{R}^3 \times S^2$. Such an image $\mathcal{U}$ can now be enhanced. Throughout this article we consider DTI-data as the initial condition, which means that we set $\mathcal{U}(\mathbf{y},\mathbf{n}) = \mathbf{n}^T\mathbf{D}(\mathbf{y})\mathbf{n}$.

2.2 Kernels for contextual enhancing of orientation distribution functions

Duits et al. [13, 17] proposed a kernel implementation that solves the diffusion equation for HARDI images. The full derivation is beyond the scope of this manuscript. This kernel represents the Brownian motion kernel, on the coupled space $\mathbb{R}^3 \rtimes S^2$ of positions and orientations. Next, we present a close analytic approximation of the Green's function. This approximation is a product of two $2D$ kernels on the coupled space $p_{2D} : \mathbb{R}^2 \rtimes S^1 \to \mathbb{R}^+$ of 2D-positions and orientations:

$$\begin{aligned} &p_{3D}^{D_{33},D_{44},t}((x,y,z)^T,\mathbf{n}(\beta,\gamma)) \approx \\ &N(D_{33},D_{44},t)\ \cdot\ p_{2D}^{D_{33},D_{44},t}((z/2,x),\beta)\ \cdot p_{2D}^{D_{33},D_{44},t}((z/2,-y),\gamma)\ , \end{aligned} \tag{4}$$

where $\mathbf{y} = (x,y,z)^T$, $N(D_{33},D_{44},t) \approx \frac{8}{\sqrt{2}}\sqrt{\pi}t\sqrt{tD_{33}}\sqrt{D_{33}D_{44}}$ takes care that the total integral over positions and orientations is 1.

The $2D$ kernel is given by:

$$p_{2D}^{D_{33},D_{44},t}(x,y,\theta) \equiv \frac{1}{32\pi t^2 c^4 D_{44} D_{33}} e^{-\frac{\sqrt{\mathrm{EN}((x,y),\theta)}}{4c^2 t}} \tag{5}$$

where we use short notation

$$\begin{aligned} EN((x,y),\theta) = &\left(\frac{\theta^2}{D_{44}} + \frac{\left(\frac{\theta y}{2} + \frac{\theta/2}{\tan(\theta/2)}\,x\right)^2}{D_{33}}\right)^2 \\ &+ \frac{1}{D_{44}D_{33}}\left(\frac{-x\theta}{2} + \frac{\theta/2}{\tan(\theta/2)}\,y\right)^2 \end{aligned}$$

where one can use the estimate $\frac{\theta/2}{\tan(\theta/2)} \approx \frac{\cos(\theta/2)}{1-(\theta^2/24)}$ for $|\theta| < \frac{\pi}{10}$ to avoid numerical errors. c is a positive constant for rescaling the diffusion time t. For details adhere to the work of Duits et al. [13, 17] and Rodrigues et al. [14].

The diffusion parameters D_{33} and D_{44} and stopping time t allow the adaptation of the kernels to different purposes:

1. $t > 0$ determines the overall size of the kernel, i.e., how relevant is the neighborhood;
2. $D_{33} > 0$, the diffusion along the principal axis, determines the width of the kernel;

3. $D_{44} > 0$ determines the angular diffusion, so the quotient D_{44}/D_{33} models the bending of the fibers along which diffusion takes place.

We can now convolve this kernel with the ODF image $\mathcal{U}$, using the HARDI convolution [14], as expressed in equation 6. We chose the parameters for the kernel in order to give a high relevance to the diffusion along the principal axis $D_{33} = 0.6, D_{44} = 0.01$ and $t = 1.4$.

$$\Phi(\mathcal{U})[\mathbf{y}, \mathbf{n}_k] = \sum_{\mathbf{y}' \in P} \sum_{\mathbf{n}' \in T} p_{\mathbf{y},\mathbf{n}_k}(\mathbf{y}', \mathbf{n}') \mathcal{U}(\mathbf{y}', \mathbf{n}') \ \Delta\mathbf{y}' \, \Delta\mathbf{n}' \tag{6}$$

where $p_{\mathbf{y},\mathbf{n}_k}$ is a kernel at position $\mathbf{y}$ and orientation $\mathbf{n}_k$, such that

$$p(R^T_{\mathbf{n}'}(\mathbf{y} - \mathbf{y}'), R^T_{\mathbf{n}'}\mathbf{n}_k) = p_{\mathbf{y},\mathbf{n}_k}(\mathbf{y}', \mathbf{n}') \tag{7}$$

and $R_{\mathbf{n}}$ is any rotation such that $R_{\mathbf{n}}\mathbf{e}_z = \mathbf{n}$. $\Delta\mathbf{y}'$ is the discrete volume measure and $\Delta\mathbf{n}'$ the discrete surface measure, which in case of (nearly) uniform sampling of the sphere, such as tessellations of icosahedrons, can reasonably be approximated by $\frac{4\pi}{|T|}$. P is the set of lattice positions neighboring to $\mathbf{y}$ and T is the set of tessellation vectors. The convolution with such a kernel will result on the extrapolation of crossing profiles where the neighborhood information so indicates, i.e., the E-ODFs.

In order to achieve the desired results, care should be taken on the sharpness of the input image $\mathcal{U}$. Before applying the convolution, the ODFs are min-max normalized and sharpening is applied by a nonlinear transformation (i.e., power of 2) of the ODFs.

2.3 Data

Synthetic Data - To validate and analyse our methodology artificial datasets were generated. DT datasets were created where two fiber bundles forming "tubes" with radii of 2 voxels intersect each other. Here, the tensors, with eigenvalues $\lambda = [17, 3, 3] \times 10^{-3} mm^2/s$ and oriented tangentially to the center line of the tube, are estimated using a mixed tensor model [5]. Gaussian noise with different SNRs is added to the real and complex part of the signal reconstructed from equation 1. In order to evaluate the angular resolution we vary the angle between the two fiber tubes $\theta \in \{50°, 60°, 70°\}$. We made a choice for these angles, given that the accuracy of Qball to detect multiple fiber orientations is around 60° [15, 18]. With these angle configurations we create two sets of data, with different acquisition parameters.

1. To evaluate the accuracy of E-ODFs we crate datasets with $b = 1000 s/mm^2$ and 49 gradient directions. We add Rician noise with SNR=20, given that this is the SNR found in literature for DTI acquisitions [2, 19]. From these datasets we estimate E-ODFs and Qballs without regularization.
2. To compare with the Qball's best case scenario, as report by Descoteaux et al. [15], we create datasets at $b = 3000 s/mm^2$ and 121 gradient direction. Since this kind of data is expected to have lower SNR, we add Rician

noise with $SNR = 10$. We estimate Qballs for these datasets and regularize with Laplace-Beltrami (LB) smoothing with $\lambda = 0.006$. This choice for the regularization parameter λ was made, since it was found to be the best at $b = 3000s/mm^2$ [15].

In order to evaluate the robustness to noise, we fix the angle to θ=70°, and we vary the SNR $\{5, 10, 20\}$. We make the same choices for b-values and number of gradients as previously described, and apply LB smoothing for the Qballs at $b = 3000s/mm^2$

Real Human Data **-** Diffusion acquisitions were performed using a twice focused spin-echo echo-planar imaging sequence on a Siemens Allegra 3T scanner, with FOV 208×208 mm, isotropic voxels of 2mm. 10 horizontal slices were positioned through the body of the *corpus callosum* and *centrum semiovale*. Uniform gradient direction scheme with 49 and 121 directions were generated with the electrostatic repulsion algorithm [20] and the diffusion-weighted volumes were interleaved with b_0 volumes every 12^{th} scanned gradient direction. Datasets were acquired at b-values of 1000 s/mm^2 and 3000 s/mm^2.

2.4 Analysis of synthetic data

To analyze the accuracy of the E-ODFs compared to the Qballs in the synthetic data sets, we calculate the angular error and standard deviation of the voxels in the crossing region. We do not expect to obtain exactly the same profile, notwithstanding it should contain the same information concerning the amount of fiber populations and their angle. To do so, we use a simple scheme for determining the error between the detected maxima, and then report the angular difference between these maxima and the simulated (true) fiber directions. We detect the maxima as the local maxima of the normalized [0,1] profiles where the function surpasses a certain threshold (here, we use 0.5). To minimize the error related to the sphere tessellation, we use 4^{th} order of tessellation of an icosahedron.

2.5 Analysis of human data

For qualitative analysis of the real data, we select an interesting region, the *centrum semiovale* (CS), where crossings are to be expected. This is a challenging region for DW-MRI analysis techniques, since fibers of the *corpus callosum* (CC), *corona radiata* (CR), and *superior longitudinal fasciculus* (SLF) form a three-fold crossing. A region-of-interest (ROI) was defined on a coronal slice (see figure 5(a)). We only do qualitative analysis for the real data, as we do not know the ground truth there.

3 Results

3.1 Phantom data results

The quantitative results of the found angular error and standard deviation of the different profiles in the crossing area from the synthetic data are presented in

Acquisition	Profiles	50°			60°			70°		
		l=4	*l=6*	*l=8*	*l=4*	*l=6*	*l=8*	*l=4*	*l=6*	*l=8*
b=1000s/mm² *NG=49; SNR=20*	*E-ODF*	x			55.5°; 12°			12°; 5°		
	Qball	x	x	x	x	54.3°; 15°	37.9°; 21°	x	43°; 25.1°	24,4°; 7.5°
b=3000s/mm² *NG=121; SNR=10*	*Regularized Qball*	x	x	37.6°; 19.9°	x	38.5°; 26.9°	33°; 27°	14.1°; 32.1°	5.4°; 3°	19°; 31°

Table 1. Table of angular error and standard deviation of the different profiles in the crossing area of the synthetic data.

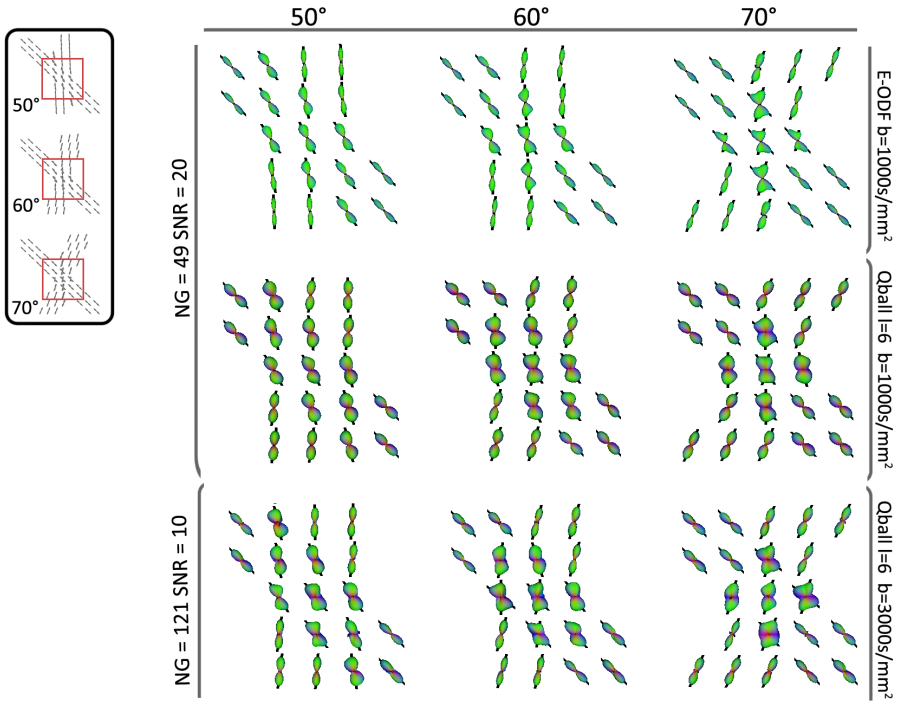

Fig. 2. E-ODFs and Qballs for different angles of crossing at fixed $SNR = 20$ for $b = 1000s/mm^2$, and SNR=10 for $b = 3000s/mm^2$. The Qballs at $b = 3000s/mm^2$ are regularized with LB smoothing with $\lambda = 0.006$.

table 1. In the following paragraphs we relate them to some figures of interesting parameter configurations and discuss the results. In figure 2, we present the results of the performance of the proposed E-ODFs compared to the Qballs [15] for different angles of crossings, and different simulation parameters: 49 gradient directions, b-value 1000 s/mm^2 and SNR 20, (figure 2 middle row) ; 121 gradient directions, b-value 3000 s/mm^2, LB smoothing with $\lambda = 0.006$ [15] and SNR 10 (figure 2 third row).

We observe that for the angle of 50°, E-ODFs and not regularized Qballs fail to find multiple maxima in the crossing areas. Only regularized Qball at high $b = 3000s/mm^2$ and high order $l = 8$, detects multiple maxima. For the

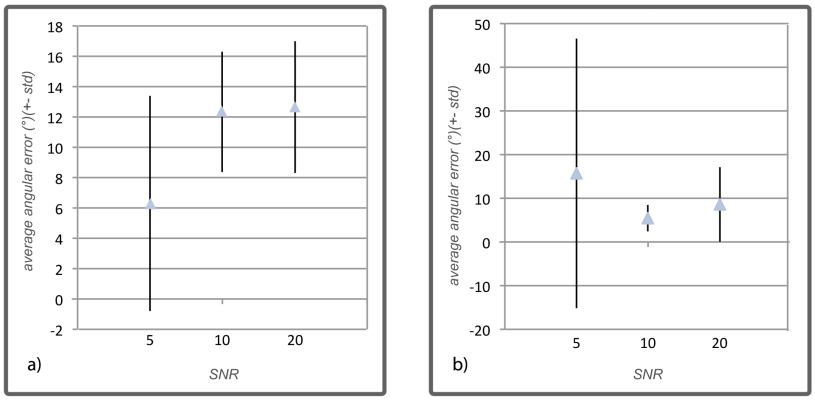

(a) (b)

Fig. 3. Angular error and standard deviation for (a) E-ODFs at $b = 1000s/mm^2$ and 49 gradient directions (b) Regularized Qball with $\lambda = 0.006$, $b = 3000s/mm^2$ and 121 gradient directions.

angle of 60° the performance of E-ODFs is similar to the un-regularized Qball at $b = 1000s/mm^2$ and truncated at order of spherical harmonics $l = 6$. Regularized Qballs at $b = 3000s/mm^2$ outperform in this scenario. At an angle of 70°, the E-ODFs outperform the best (un-regularized) Qball scenario at order $l = 8$. Only regularized Qball at $l = 6$ outperforms in this scenario (see table of figure 1).

The plots of figure 3.1 report the relation between the angular error and change in SNR. We observe that the E-ODFs are more stable, regardless the noise level, whereas the regularized Qballs improve significantly at higher SNRs. However, it is important to note that in real data at high b-value $\approx 3000s/mm^2$ the SNR drops off to 5 (however, this might change depending on the type of scanner and imaging parameters). Figure 4 illustrates the previous conclusions. At higher order of truncation un-regularized Qball performs much worse, giving many false positives in the linear areas where the SNR is low.

We observe that regardless the SNR, the E-ODFs preserve the coherence of the linear and crossing regions, and preserve the angular error, to almost constant (see figure 3(a)). We also compared the E-ODFs, to Qball's best case scenario with LB regularization [15]. Here, for SNR 5, Qball performs worse (angular error of 14.9° and standard deviation 8.4°) than the E-ODFs. As noise decreases, E-ODFs' performance is similar to the regularized Qballs at $b = 3000s/mm^2$ (angular error 9.8° and standard deviation 9.15°). Regularized Qball outperforms E-ODFs, for SNR 20, with an angular error of 5.15° and standard deviation of 3.2°. However, this SNR is not realistic given nowadays acquisition protocols and machinery at b-values as high as $3000s/mm^2$.

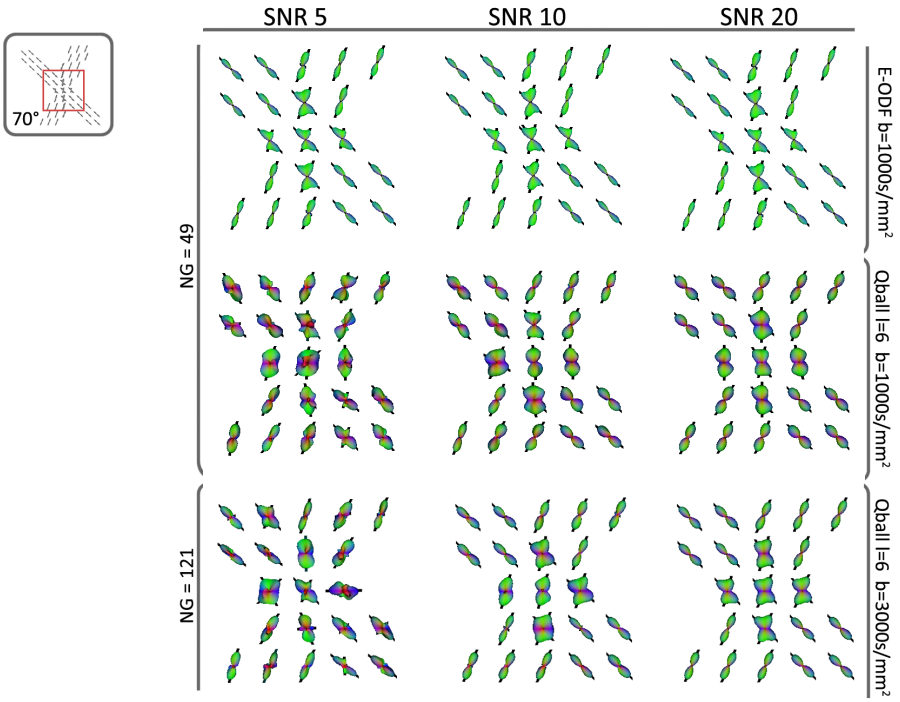

Fig. 4. E-ODFs and Qballs for different SNRs, and different b-value, at fixed angle of 70°.

3.2 Real data results

Even though crossing information is missing in the original DTI data, as well as in the created ODFs (as can be seen in figure 5(a) and figure 5(b)), we observe that after processing, crossing information is extrapolated (see figure 6(c)). The obtained crossings are very much comparable to the Qball reconstructions of $l = 6$, at $b = 3000s/mm^2$ and 121 gradient directions and regularized with LB smoothing of $\lambda = 0.006$ (figure 6(b)). The un-regularized Qballs at low b-value of $1000s/mm^2$ and low gradient sampling of 49 gradient directions, present less obvious structures of the CC and CR, and have more chaotically oriented crossings, figure 6(a).

All computations were conducted in an AMD Athlon X2 Dual 2.41GHz, with 3GB of RAM, taking 0.5 minutes per artificial tube dataset, and about 13 minutes for the real human brain dataset for estimating the E-ODFs.

4 Conclusions and Future Work

In this work we presented a method for extrapolating crossing information using image processing of the coupled space of positions and orientations in DTI data.

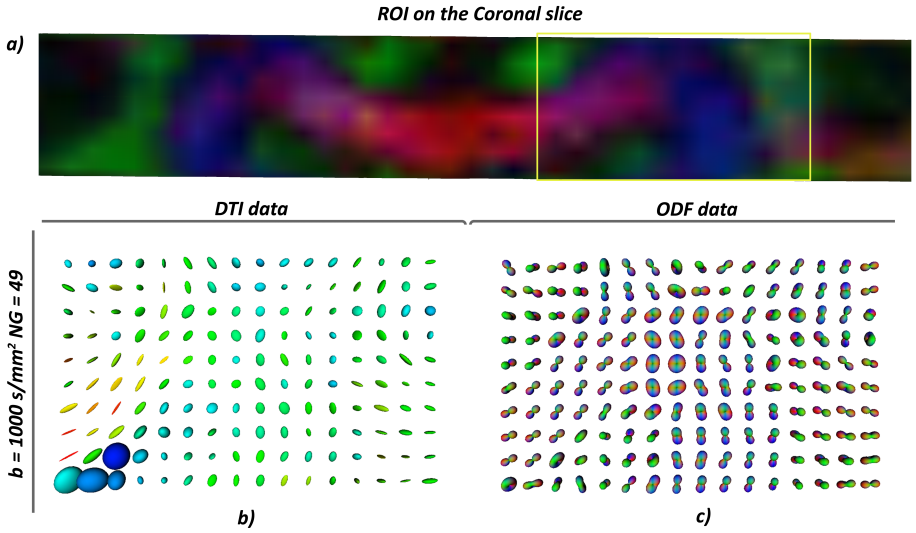

Fig. 5. The *centrum semiovale*. Left: the original DTI data, color coded by FA. Right: the ODFs from the DTI data, RGB color coded by orientation and min-max normalized.

We show that with typical acquisition schemes for DTI, the inferred fiber crossings are similar to the crossings from 6^{th} order un-regularized Qball estimated from the same data. Furthermore we compare the E-ODFs to the best scenario of Qball at typical HARDI acquisition schemes, and we conclude that the information gain from the regularized Qball is similar at low SNR, but the Qballs improve when increasing the SNR. However, in practice HARDI acquisitions at high b-values result in very noisy datasets, and Qball reconstructions of poor quality including LB regularization. The robustness to noise of the presented method is significantly better than from the un-regularized Qballs reconstructed from the same data, and comparable to the Qball's best scenario. The main contribution from this work lies on demonstrating similar quality of detected crossings with modest acquisitions modeled by DTI, and with the use of contextual information as in the popular HARDI reconstruction techniques that require more expensive acquisitions such as Qball. Future work addresses similar comparison to spherical deconvolution [8] as well as tensor decomposition techniques [21] which has proven to more reliably infer number and directions of fibers. The chosen kernel sets an overall reasonable probabilistic model that governs how the context of a fiber fragment is taken into account. Consequently, our framework lacks adaptivity. Future work will address more adaptive fiber context models to the data, such that context is only included where it is required by the data.

The method proposed has its limitations, it assumes that enough context is available for a correct extrapolation. The possible implications of this limitations for concrete brain structures should be studied. Future work should additionally bear more extensive validation to assess the exact differences between HARDI

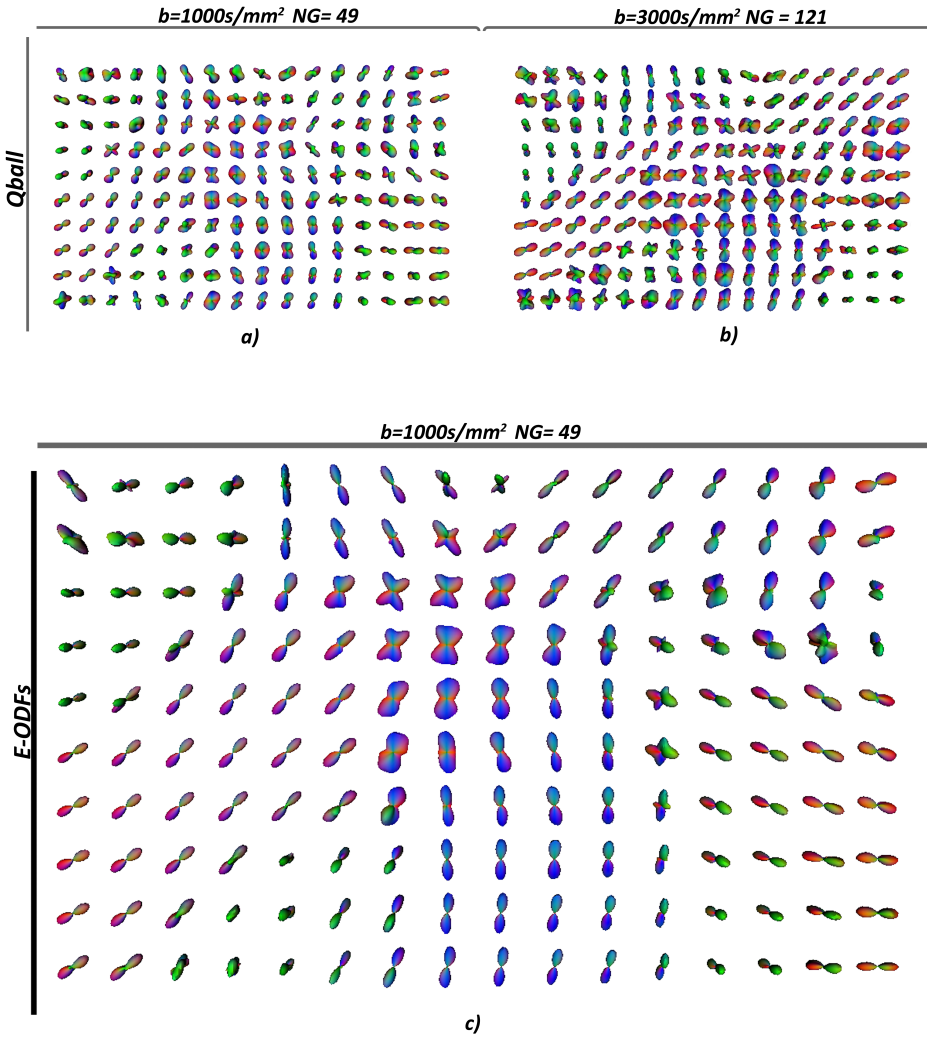

Fig. 6. Different profiles in the *centrum semiovale* a) un-regularized Qball of order 4 b) Regularized Qball with $\lambda = 0.006$ of order 6 from similar region as (a) c) E-ODFs of the same region as (a).

models and E-ODFs concerning acquisition parameters and anatomical areas of the brain. This includes synthetic data experiments with fibers of different configurations (e.g. curved bundles) and multiple crossings. As a conclusion, contextual processing of DTI data allows overcoming one of the main drawbacks of the DT model. The crossing information can be recovered with an acquisition that typically takes 3-6 minutes and modest post-processing (13 minutes for 10

slices of a human brain on a standard PC). This gives future work potential for applying more accurate stream-based tractography for DTI data.

References

1. Basser, P.J., Mattiello, J., Lebihan, D.: MR diffusion tensor spectroscopy and imaging. Biophys. J. **66**(1) (January 1994) 259–267
2. Jones, D.K.: The effect of gradient sampling schemes on measures derived from diffusion tensor mri: a monte carlo study. MRM **51**(4) (2004) 807–15
3. Tuch, D.S.: Diffusion MRI of complex tissue structure. PhD thesis, Harvard (2002)
4. Frank, L.R.: Characterization of anisotropy in high angular resolution diffusion-weighted MRI. MRM **47**(6) (2002) 1083–99
5. Alexander, D.C., Barker, G.J., Arridge, S.R.: Detection and modeling of non-gaussian apparent diffusion coefficient profiles in human brain data. MRM **48**(2) (2002) 331–40
6. Tuch, D.: Q-ball imaging. MRM **52** (2004) 1358–1372
7. Özarslan, E., Shepherd, T.M., Vemuri, B.C., Blackband, S.J., Mareci, T.H.: Resolution of complex tissue microarchitecture using the diffusion orientation transform (DOT). NeuroImage **36**(3) (July 2006) 1086–1103
8. Tournier, J.D., Calamante, F., Connelly, A.: Robust determination of the fibre orientation distribution in diffusion MRI: non-negativity constrained super-resolved spherical deconvolution. NeuroImage **35**(4) (2007) 1459–72
9. Jian, B., Vemuri, B.C.: A unified computational framework for deconvolution to reconstruct multiple fibers from Diffusion Weighted MRI. IEEE Transactions on Medical Imaging **26**(11) (2007) 1464–1471
10. Descoteaux, M.: High Angular Resolution Diffusion MRI: From Local Estimation to Segmentation and Tractography. PhD thesis, Universite de Nice - Sophia Antipolis (February 2008)
11. Liu, C., Bammer, R., Acar, B., Moseley, M.E.: Characterizing non-gaussian diffusion by using generalized diffusion tensors. MRM **51**(5) (2004) 924–37
12. A. Barmpoutis, B. C. Vemuri, D.H., Forder, J.R.: Extracting tractosemas from a displacement probability field for tractography in DW-MRI. In LNCS 5241, MICCAI (6-10 September 2008) 9–16
13. Duits, R., Franken, E.: Left-invariant diffusions on $\mathbb{R}^3 \rtimes S^2$ and their application to crossing-preserving smoothing on HARDI-images. CASA report, TU/e, nr.18
14. Rodrigues, P.R., Duits, R., ter Haar Romeny, B., Vilanova, A.: Accelerated diffusion operators for enhancing DW-MRI. In: VCBM, Leipzig, Germany (2010)
15. Descoteaux, M., Angelino, E., Fitzgibbons, S., Deriche, R.: Regularized, fast and robust analytical Q-Ball imaging. MRM **58** (2007) 497–510
16. Basser, P.J., Mattiello, J., Lebihan, D.: Estimation of the effective self-diffusion tensor from the NMR spin echo. J. of Magn. Res. **Series B 103** (1994) 247–254
17. Duits, R., Franken, E.: Left-invariant diffusions on the space of positions and orientations and their application to crossing-preserving smoothing of HARDI images. International Journal of Computer Vision 2010
18. Prčkovska, V., Roebroeck, A.F., Pullens, W., Vilanova, A., ter Haar Romeny, B.M.: Optimal acquisition schemes in high angular resolution diffusion weighted imaging. In: MICCAI. Volume 5242 of LNCS., Springer (2008) 9–17
19. Lagana, M., Rovaris, M., Ceccarelli, A., Venturelli, C., Marini, S., Baselli, G.: DTI parameter optimisation for acquisition at 1.5T: SNR analysis and clinical application. Comput Intell Neurosci **NIL**(NIL) (2010) 254032
20. Jones, D., Horsfield, M., Simmons, A.: Optimal strategies for measuring diffusion in anisotropic systems by magnetic resonance imaging. MRM **42** (1999) 515–525
21. Schultz, T., Seidel, H.P.: Estimating crossing fibers: A tensor decomposition approach. IEEE Transactions on Visualization and Computer Graphics **14** (2008) 1635–1642